Future changes in the influence of the NAO on Mediterranean winter precipitation extremes in the EC-Earth3 large Ensemble: The prominent role of internal variability

Atmospheric Research 304 (2024) 107391

Contents lists available at ScienceDirect

Atmospheric Research

journal homepage: www.elsevier.com/locate/atmosres

Future changes in the influence of the NAO on Mediterranean winter precipitation extremes in the EC-Earth3 large Ensemble: The prominent role of internal variability

Andrea Rivosecchi [a,b,c], M.A. Bollasina [a,*], I. Colfescu [d]

[a] School of GeoSciences, University of Edinburgh, Edinburgh, UK
[b] Impacts on Agriculture, Forestry and Ecosystem Services (IAFES) Division, Euro-Mediterranean Center on Climate Changes (CMCC), Sassari, Italy
[c] National Biodiversity Future Center (NBFC), Palermo, Italy
[d] National Centre for Atmospheric Science, UK

ARTICLE INFO

Keywords:
North Atlantic oscillation
Precipitation extremes
Projections
Internal variability

ABSTRACT

One of the largest uncertainties in future climate projections is the interplay between internally generated and externally forced changes. This study investigates the changes in the link between the North Atlantic Oscillation (NAO) and Mediterranean winter extreme rainfall and dry days by the end of the 21st century compared to present day. We compare two different future pathways and estimate the extent to which the NAO imprint is affected by the global warming level using the latest EC-Earth3 large ensemble historical and future experiments. It is shown that the expected range of winter extremes changes due to internal and unpredictable fluctuations of the NAO largely overcomes the signal associated with externally-forced NAO variations. The NAO is found to exert a similar control on European climate variability, regardless of the amount of warming. For most of the Mediterranean region, magnitude and even sign of projected changes in the NAO-congruent precipitation indices vary substantially across the individual ensemble members according to the corresponding evolution of the NAO. Internal variability provides an average basin-wide contribution of up to 90% or more to the total NAO-driven variability in SSP1–1.9, and of about 80% in SSP5–8.5. Sub-regionally, the anthropogenic component of the NAO link is more evident over the Iberian Peninsula and parts of the central Mediterranean. This emphasises the role of internal variability and related uncertainty in determining the future impact of the NAO via the large spread in the circulation responses. However, the NAO is found to exert a weaker influence on the extreme precipitation total variability in both future scenarios given their future marked increase in total intensity and variance as opposed to the negligible NAO-related trends. Opposite conclusions are drawn for dry days, which are projected to decrease in the future, especially in the northern Mediterranean. Thus, this study also highlights how the variability of future extreme precipitation intensity in the Mediterranean basin will be less dependent on the principal mode of internal climate variability, posing further challenges for prediction and adaptation to weather-related hazards.

1. Introduction

Although a worldwide increase in human and economic losses related to climate change is expected in the future, global warming will not have a geographically homogenous impact. The Mediterranean basin is considered a climate change "hotspot" as it is particularly vulnerable to the future intensification of climate-related hazards (Cramer et al., 2018; Tuel and Eltahir, 2020). The region is already undergoing progressive aridification caused by the concomitant, basin-wide increase in average temperatures and the reduction in precipitation rates (e.g., Giorgi and Lionello, 2008; Sillmann et al., 2013). The latter is opposed to the observed increase in the frequency and intensity of extreme precipitation events (Alpert et al., 2002). This is of particular concern, as extreme rainfall is strongly correlated with the occurrence of floods (Madsen et al., 2014), which have produced dramatic losses across southern Europe and the Mediterranean (Svetlana et al., 2015;

* Corresponding author at: School of GeoSciences, The University of Edinburgh, Crew Building, The King's Buildings, Alexander Crum Brown Road, Edinburgh EH9 3FF, UK.
E-mail address: Massimo.Bollasina@ed.ac.uk (M.A. Bollasina).

https://doi.org/10.1016/j.atmosres.2024.107391
Received 16 January 2024; Received in revised form 15 March 2024; Accepted 1 April 2024
Available online 2 April 2024

Sassi et al., 2019; EEA, 2022).

Despite mean drier conditions, heavy precipitation is projected to increase over many parts of southern Europe and the Mediterranean under global warming (Sillmann et al., 2013; Chen et al., 2014; Giorgi et al., 2014). For example, Vautard et al. (2014) found a robust and widespread increase (5–15%) in heavy precipitation in winter but only a modest and spatially confined mean wetting at +2 °C warming. In contrast, no changes were found in summer extreme precipitation despite the marked mean drying. Polade et al. (2017) showed a 10–40% decrease in the average precipitation intensity as opposed to a 10% increase in the intensity of extreme precipitation by 2060–2090 compared to present day. Accordingly, Zittis et al. (2021) pointed out how precipitation extremes will contribute to a larger (5–30%) share of the total Mediterranean precipitation by the end of the century. King and Karoly (2017) found a 4–6% increase in extreme one-day precipitation amounts over most of southern Europe in summer and winter at +2 °C compared to +1.5 °C global warming levels. These studies suggest that although dry conditions become more severe, precipitation can be much more extreme when it does occur.

However, there is still considerable uncertainty in quantifying the importance of individual drivers of these changes. The human-induced rise in global mean temperatures is unequivocally the predominant driver of recent climate change (IPCC, 2021). Based on observations and climate models, Myhre et al. (2019) found total precipitation from intense events to almost double per degree of warming. This is particularly evident in Europe (Myhre et al., 2019; Fischer and Knutti, 2016), consistently with some of the studies mentioned above. Despite the importance of thermodynamically-driven precipitation changes resulting from anthropogenic warming and moistening of the atmosphere, atmospheric dynamics remains a significant controller of weather patterns and extremes (e.g., Pfahl et al., 2017), particularly over the Mediterranean. Yet, significant disparities between the observed and simulated circulation variability have been recently described, particularly over the North Atlantic during winter (e.g., Kravtsov, 2017), and its role in future climate projections is generally underestimated (e.g., O'Reilly et al., 2021). As such, internal climate variability generates large uncertainties around the externally-forced signal (Deser et al., 2012; Wallace et al., 2013; Shepherd, 2014; O'Reilly et al., 2021). For regional precipitation, internal variability dominated the late 20th-century drying (Kelley et al., 2012) and might remain dominant through the middle of the 21st century (Lehner et al., 2020). The extent to which future climate will depend on the interaction between anthropogenic forcing and internal climate variability has thus been the focus of recent publications (Suarez-Gutierrez et al., 2018; Wood and Ludwig, 2020; Yu et al., 2020; Blanusa et al., 2023).

In the Northern Hemisphere, the primary mode of internal climate variability is the North Atlantic Oscillation (NAO; Hurrell, 1995). Extensive evidence documents the influence of the NAO interannual and interdecadal variability on average precipitation and temperature patterns across Europe (Tomozeiu et al., 2002; Dünkeloh and Jacobeit, 2003; Knippertz et al., 2003; Trigo et al., 2004). This link is stronger in winter, when the NAO explains ~35% of the total temperature and pressure variance (Hurrell, 1995; Hurrell and Deser, 2010). When the pressure gradient between the centres of action is enhanced (positive NAO), wetter, warmer conditions develop in north-western Europe as opposed to a colder, drier climate in the Mediterranean (e.g., Castro-Díez et al., 2002). Additionally, NAO variability also entails a variation in the relative spatial position of the two action centres (Rousi et al., 2017) as well as a longitudinal tilt of its axis (Luo et al., 2015; Yao et al., 2016) modulating the effects produced by the NAO temporal variability and leading to downstream extreme events (Jung et al., 2003; Yao et al., 2016; Rousi et al., 2020).

The influence of historical NAO variability on Mediterranean climate extends to weather extremes, with a consensus on a significant anti-correlation between the winter NAO and the intensity and frequency of extreme precipitation. Yet, most studies analyse this link on sub-regional scales (Houssos and Bartzokas, 2006; Queralt et al., 2009; Tramblay et al., 2012; Ferrari et al., 2013; Corona et al., 2018; Luppichini et al., 2021), with basin-wide approaches being much less common (e.g., Krichak et al., 2014).

Mediterranean climate over the coming decades will continue to be influenced by the NAO, and it is critical to understand how this relationship might evolve under increasing global warming. Although the NAO is an intrinsic mode of atmospheric circulation variability, its characteristics may be altered directly or indirectly by external forcing (e.g., via changes in North Atlantic and tropical SSTs; Visbeck et al., 2001; Tao et al., 2023). The latest CMIP5/CMIP6 models generally agree in projecting a strengthening of the winter NAO by the late 21st century (Gillett and Fyfe, 2013; Deser et al., 2017; Fabiano et al., 2021; Lee et al., 2021; McKenna and Maycock, 2022), in conjunction with spatial rearrangement of its poles (Rousi et al., 2020). This would result in a NAO-related mean precipitation decrease in the Mediterranean (e.g., Lopez-Moreno et al., 2011; Deser et al., 2017; Lee et al., 2021), exacerbating the projected externally-forced drying (e.g., Cos et al., 2022). Future atmospheric circulation changes have been identified as the predominant contributors to mean Mediterranean precipitation variations and their future uncertainties (Zappa et al., 2015; Zappa and Shepherd, 2017; Tuel et al., 2021). The current generation of coupled climate models struggles to reproduce the NAO contribution to multidecadal climate trends (Smith et al., 2020; Ballinger et al., 2023). Importantly, uncertainties in the NAO intrinsic dynamics constitute a major source of discrepancies in future projections of regional climate (e.g., Deser et al., 2017; Fereday et al., 2018; McKenna and Maycock, 2021), particularly for mean wintertime precipitation over southern Europe (McKenna and Maycock, 2021).

This study aims to build on previous works, particularly Deser et al. (2017) and McKenna and Maycock (2021), and to extend their results by 1) assessing the historical influence of NAO variability on precipitation extremes across the whole Mediterranean basin; 2) expanding this analysis to projections for the end of the 21st century, investigating how the relationship might change at different levels of global warming; 3) quantifying the contribution of internal variability to the future changes and its interplay with external forcing. Using a very large initial condition ensemble provides a more accurate measure of the forced climate response while more robustly accounting for the role of internal variability compared, for example, to using the common CMIP5/6 ensembles.

2. Data and methods

This study uses data from large-ensemble (50 members) experiments carried out with the EC-Earth3 earth system model (Döscher et al., 2022). Historical (1850–2014) simulations and 21st century projections (2015–2100) under two different shared socio-economic pathways (SSPs), namely SSP1–1.9 and SSP5–8.5, are analysed. SSP1–1.9 represents the low end of global warming trends, with greenhouse gas emissions reaching net zero by 2050 to achieve a maximum warming of 1.5 °C by 2100 compared to pre-industrial times. Conversely, SSP5–8.5 is the "business as usual" scenario in which emission rates remain constant leading to an end-of-century global surface air temperature rise of +5 °C since the pre-industrial times (O'Neill et al., 2014). These two opposite scenarios allow us to contrast the impact of very different anthropogenic radiative forcing estimates on the NAO-extremes relationship, with the end-of-century interval highlighting the largest difference between them (resulting from the spread in both greenhouse gas and regional anthropogenic aerosol emissions). Note that EC-Earth3 provides the largest and highest-resolution ensemble among the other models participating in the Multi-Model Large Ensemble Archive initiative (Deser et al., 2020). Relevant to this study, EC-Earth3 shows good skill among the CMIP5/6 models in simulating the NAO and its relationship with mean and extreme precipitation over the North Atlantic (see also the Supplementary Material for more details on the

model and Fig. S1). Present-day is the 1979–2008 period, while the future is the 30-year period (2071–2100).

For validation purposes, the present-day simulated NAO and extreme precipitation indices are compared to their observational counterpart, derived, respectively, from the European Centre for Medium Range Weather Forecast Reanalysis version 5 (ERA5; Hersbach et al., 2020) and the Ensembles daily gridded Observational dataset for precipitation in Europe version 23.1 (EOBS23.1), both at 0.25° horizontal resolution (Cornes et al., 2018).

The NAO is defined by an Empirical Orthogonal Function (EOF) analysis of monthly 500-hPa geopotential height anomalies (from the present-day climatology) over the North Atlantic domain (20°-80°N, 90°W-40°E) for the extended winter season (DJFM). The winter period is when the NAO effects on Euro-Mediterranean climate are stronger and better understood (Hurrell and Deser, 2010). The geopotential height anomalies are linearly detrended prior to the EOF calculation. The 500-hPa field is used rather than sea-level pressure since it is less affected by local meteorology (Nigam and Baxter, 2015). The NAO index is defined as the standardized principal component (PC) time series resulting from the EOF analysis (Deser et al., 2017). Note that an EOF-based NAO definition captures both its temporal as well as spatial characteristics simultaneously, while a more traditional NAO index cannot reflect the NAO spatial variations.

Daily precipitation data are used to calculate intensity and variance of precipitation extremes indices. The indices analysed here are the monthly 95th percentile of daily precipitation intensity (R95p, mm day^{-1}), the monthly highest one-day precipitation intensity (Rx1day, mm day^{-1}) and the monthly maximum number of consecutive dry days (CDD, day). All the indices are calculated according to the Expert Team on Climate Change Detection and Indices (ETCCDI) definitions (Zhang et al., 2011).

Least-squares correlation/regression analysis is used to quantify the NAO imprint using monthly values. Ensemble-mean quantities are used to identify externally forced changes, while the differences between each of the 50 ensemble members and the ensemble mean allow the separation of the role of internal variability (Deser et al., 2016). The statistical significance of the correlations is assessed at the 90% confidence level ($p = 0.1$) using the Wald Test with t-distribution of the test statistic.

A quantitative estimate of the relative importance of the forced and internal components of the projected precipitation changes can be obtained by calculating the signal-to-noise ratio (SNR; Deser et al., 2016), defined as the absolute value of the forced change represented by the ensemble mean (the signal) divided by the standard deviation (Std) of the changes across the 50 ensemble members (the noise). The contribution of internal variability to total changes (IV, %) can then be estimated as (e.g., Garcia-Martinez and Bollasina, 2021):

$$IV(\%) = \frac{Std\ x\ 100}{|Mean| + Std}$$

3. Results

3.1. Historical influence of the NAO on weather extremes

The present-day observed and simulated NAO spatial patterns are compared in Fig. 1a-b. The model provides a realistic representation of observations, with good agreement on magnitude and location of the NAO action centres. For the model, the EOF analysis has been conducted for each ensemble member separately (Fig. S2), and then averaged to obtain robust ensemble-mean patterns. Very similar results are obtained by performing a concatenated EOF analysis across the 50 ensemble members (not shown). A depiction of the 5–95% range of simulated NAO patterns (i.e., the model's uncertainty in simulating the NAO) is shown in Fig. S3. Compared to the ensemble mean, the pattern at the upper tail (the 95 percentile) features a stronger (weaker) southern

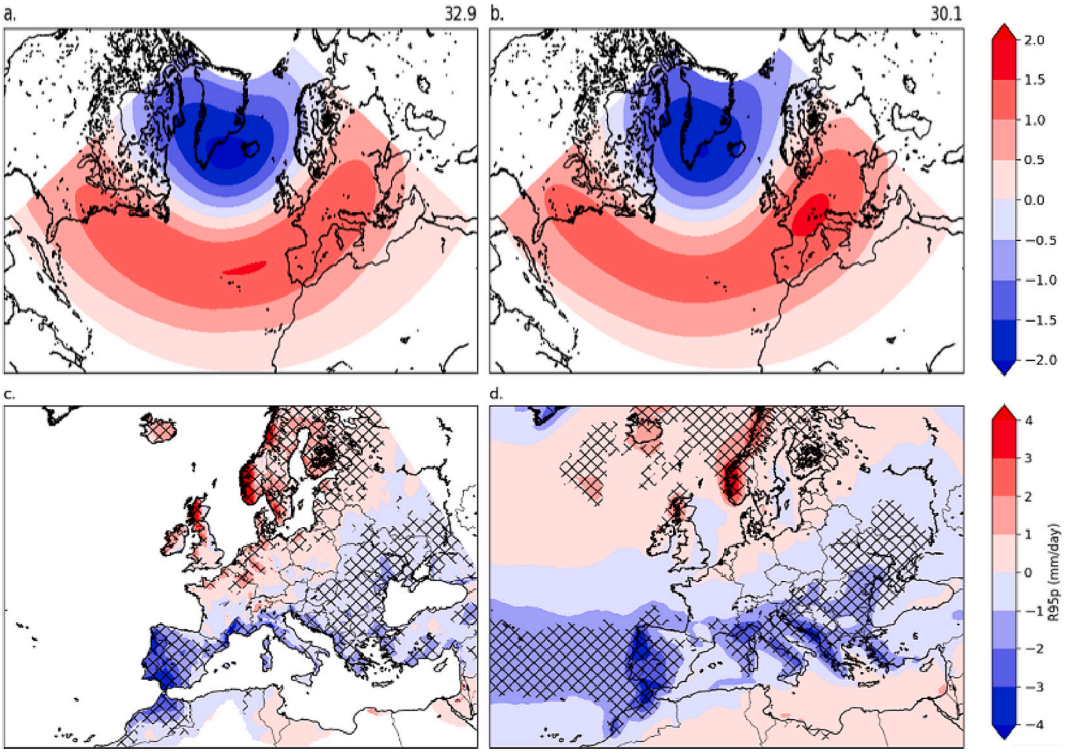

Fig. 1. Top: Historical (1979–2008) NAO pattern in (left) observations and (right) the EC-Earth3 ensemble mean for DJFM. Anomalies in a) and b) are normalised by the standard deviation of the respective principal component timeseries. The numbers indicate the percentage of variance explained by the NAO pattern. Bottom: Regressions of R95p (mm day^{-1}) on the historical NAO time series in (left) observations and (right) the EC-Earth3 ensemble mean. The cross-hatching in c) and d) marks regions where the correlation exceeds the 90% confidence level.

(northern) NAO pole and a northern shift of the NAO dipole nodal line, while the one at the lower tail shows opposite features. Overall, the model's range of NAO magnitudes and patterns span the NAO single realisation in observations. The percentage of variance explained by the leading EOF shows relatively low inter-ensemble variations (25–35%), realistically enclosing the observed variance (Fig. S2). Examining the temporal characteristics of the NAO variability, the individual members' time series display amplitudes comparable to observations but largely uncorrelated variations, resulting in a comparatively small amplitude time series in the ensemble mean (not shown). This indicates NAO variability to be almost entirely internally generated. An EOF analysis carried out on the individual members after subtracting the ensemble mean (not shown) shows irrelevant differences from the above results, further confirming the externally forced component of NAO variability to be of negligible magnitude.

Figure 1c-d display the influence of the NAO on present-day R95p over the wider European region to better interpret the Mediterranean pattern in the context of the continental-scale NAO signature. Consistently with the NAO spatial structure and associated seasonal precipitation anomalies, the observed extreme precipitation pattern features a reduction across the Mediterranean and the Balkans and an increase over most of northern Europe, the British Isles, and Scandinavia. In the Mediterranean area, the largest and more extensive anomalies are found over Iberia and northern Morocco, where the NAO-related variability amounts to even 40–80% of the climatology (see Fig. S1). Large, albeit more spatially confined, negative anomalies are found over Southern France, the western Italian coast, the Balkans, and the Aegean Sea (20–40% of the seasonal mean climatology). The latitudinal gradient in the NAO-related R95p anomalies is well captured by the ensemble mean, which realistically simulates the observed regressions in the most NAO-sensitive areas.

The range of NAO patterns shown in Fig. S2 translates into a corresponding variety of precipitation anomalies across the Mediterranean and Europe (Fig. S4). The 5–95% range of uncertainty in the R95p regressions is displayed in Fig. S5. The circulation pattern associated with the upper end of the simulated NAO range implies stronger anomalous westerly flow over northern Europe and Scandinavia, favouring enhanced precipitation there, but also weaker anticyclonic winds over the Mediterranean, where the precipitation deficit is reduced. Interestingly, the stronger southern NAO anomaly is associated with more intense northeasterlies over the southern and eastern Mediterranean, leading to precipitation increases over northern Africa. Conversely, the weaker westerly flow associated with the lower end of the NAO range leads to smaller precipitation increases over northern Europe while the north-eastward tilted circulation pattern is associated with stronger blocking across the Mediterranean and central Europe, where precipitation decreases. As a result of this uncertainty, the R95p regressions over the Mediterranean range from large negative to weak positive values.

The observed NAO-induced anomalies for Rx1day bear a close resemblance to those for R95p in the spatial distribution, while their magnitude is about 15–20% larger on average, especially over Iberia and the western Mediterranean (Fig. 2). Accordingly, the model (ensemble mean) offers a good representation of the regression sign and magnitude throughout the studied region, including the overall more pronounced meridional dipole compared to R95p (Fig. 1). The consistency between the responses of the two precipitation extreme indices extends to the individual ensemble members (not shown). Rx1day displays very similar patterns to R95p but with anomalies of larger magnitude across the Mediterranean, resulting in a much larger inter-ensemble standard deviation over the area and larger uncertainty in the individual members' response (Fig. S6). This implies that the NAO affects the two precipitation intensity indices similarly in terms of spatial pattern but with much larger variability for Rx1day compared to R95p.

The CDD regression (Fig. 2) displays a pattern largely specular to those previously assessed, with widespread positive anomalies across

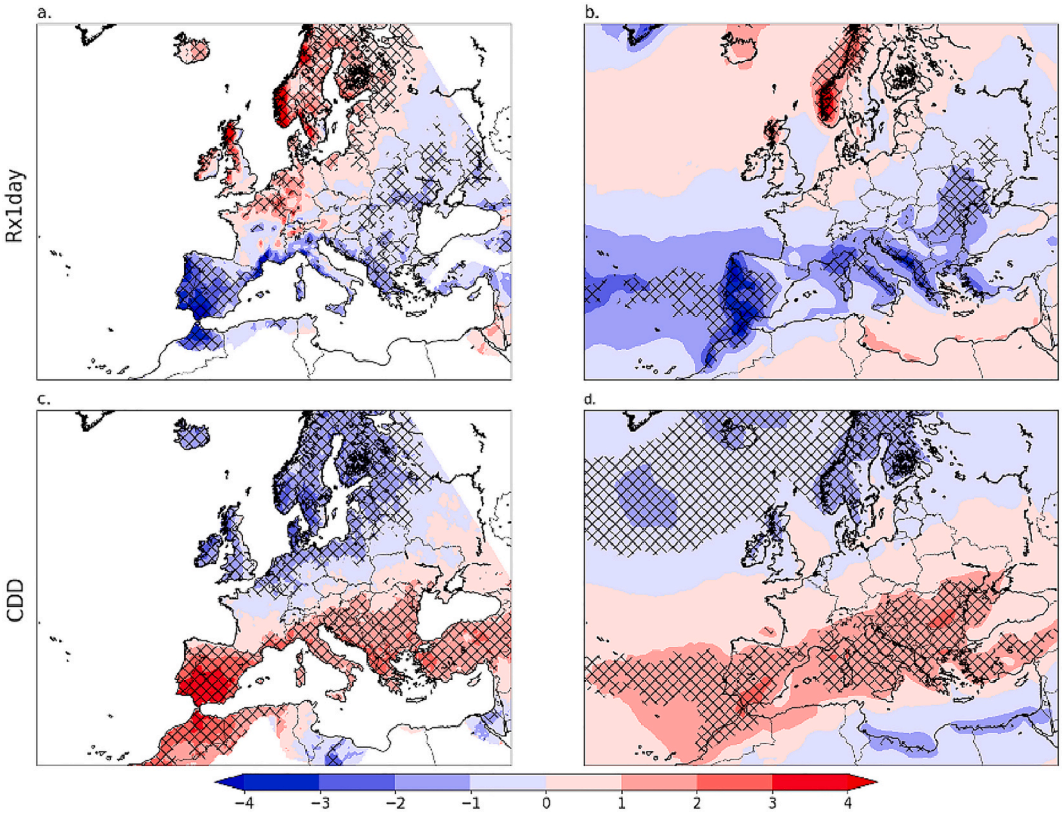

Fig. 2. Regressions of (top) Rx1day (mm day^{-1}) and (bottom) CDD (days) on the historical NAO time series in (left) observations and (right) the EC-Earth3 ensemble mean. The cross-hatching marks regions where the correlation exceeds the 90% confidence level.

the Mediterranean and southern Europe (of magnitude between 25 and 30% of the climatology), and negative anomalies at high latitudes in both observations and model. This pattern is consistent with the general effects of the NAO on European climate, with its positive phase promoting drier (wetter) conditions over southern (northern) Europe. The model reproduces observations well, albeit weaker anomalies over Spain and Morocco and more extensive drying over most of central Europe. It is worth noticing that, compared to R95p and Rx1day whose more prominent anomalies are located over western Iberia and the central Mediterranean, CDD has a more uniform and zonally oriented pattern with core anomalies over the western Mediterranean and northwestern Africa. Relative variations of pattern and magnitude of CDD anomalies across individual members (not shown) are consistent with those discussed above for R95p and Rx1day and reflect the inter-member diversity in the simulated NAO structure. As a result, the inter-member standard deviation is relatively uniform across the Mediterranean, with maxima over southern Spain, Morocco and the western Mediterranean (up to 40–50% of the ensemble mean signal). The smaller spread and larger mean signal across the Mediterranean and southern Europe, compared, for example, to R95p, lead to a 5–95% range of uncertainty which features anomalies of the same (positive) sign at both tails (Fig. S6). The link between the NAO and CDD is thus more consistent in sign across the members than that of the other precipitation indices over most of the region.

3.2. Future changes in extremes intensity and NAO influence

3.2.1. Future NAO changes

The leading mode of variability of the winter 500-hPa geopotential height anomalies during 2071–2100 for the two future scenarios is displayed in Fig. 3. While both future patterns feature the traditional NAO dipole structure over the North Atlantic, consistent with that during the historical period, a close examination reveals several important differences (Fig. S7). Both scenarios feature an anomalous tripole compared to the historical pattern, which is brought about by changes in the NAO key centres. The Icelandic low, while displaying minor variations in magnitude and location, undergoes a noticeable westward shift and a meridional contraction, particularly on its southern flank over the Atlantic. The Azores high shows an overall weakening (in SSP1–1.9) or marked westward shift (in SSP5–8.5), with, in the latter case, the largest core displaced over the mid-Atlantic basin. In both cases, markedly weaker anticyclonic anomalies occur over central Europe and the Mediterranean compared to the historical period. It is noteworthy that positive and negative centres do not vary consistently

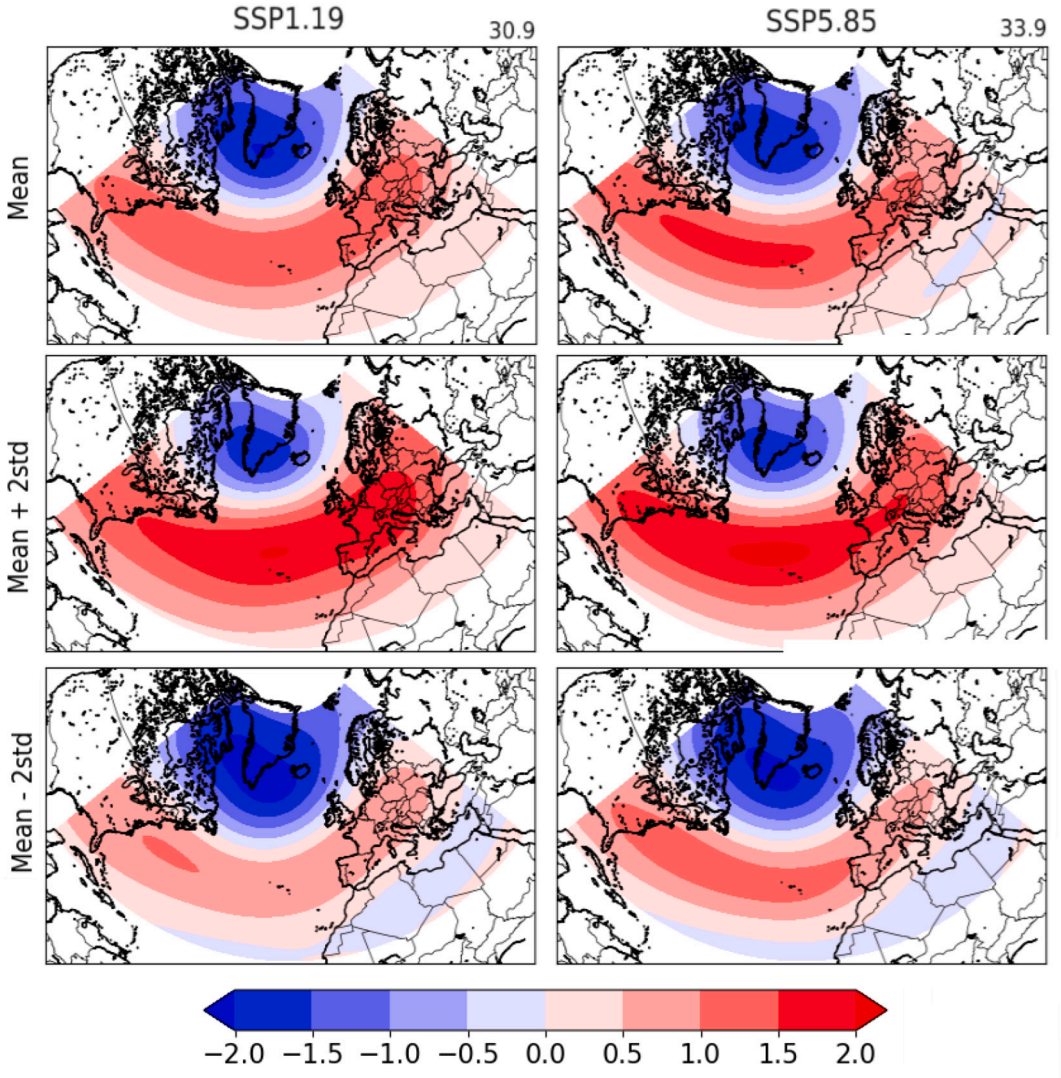

Fig. 3. Future (2071–2100) DJFM NAO patterns in the EC-Earth3 ensemble mean for (left) SSP1–1.9 and (right) SSP5–8.5. From top to bottom: the mean NAO, the 95% (mean + 2 inter-member standard deviations), and the 5% (mean - 2 inter-member standard deviations). The numbers on the top panels indicate the percentage of variance explained by the NAO pattern.

between the two scenarios: the lower warming scenario shows the largest anomalies to the west of the Icelandic Low, while changes in SSP5–8.5 are the largest for the southern centre of action (Fig. 3). This highlights an important dynamical feature of the externally-forced NAO response. The explained variance in SSP1–1.9 (30.9%) and SSP5–8.5 (33.9%) is not significantly different from that in the historical period, indicating a similar control of the NAO on mean European climate variability, regardless of the amount of warming.

Inspection of the NAO changes for individual ensemble members shows, not surprisingly, a range of patterns and magnitudes (Figs. S8 and S9). Some members display only modest differences in the NAO pattern compared to present-day (e.g., simulation 42 in SSP1–1.9 and simulation 13 in SSP5–8.5), while others show very large differences (e.g., simulation 1 in SSP1–1.9 and 40 in SSP5–8.5). Simulation 45 in SSP1–1.9 and 48 in SSP5–8.5 show a stronger northern centre of action and a weaker southern pole, while the opposite occurs for simulations 12 in SSP1–1.9 and 15 in SSP5–8.5. The variety of NAO patterns, summarized by the inter-ensemble standard deviation (not shown), exhibits a maximum core over the mid-Atlantic basin in both SSP1–1.9 and SSP5–8.5, similarly to the historical period. Yet, it is worth noting that the area of largest values is much more confined to the ocean, with generally reduced spread over Europe compared to the present day. This indicates a slightly larger inter-ensemble consistency, and thus less uncertainty, in the future NAO pattern over Europe and the Mediterranean. Additionally, the range of variance explained increases, albeit weakly, in both future scenarios compared to the historical period, due to members for which the percentage of variance reaches up to 38.7% and 40.0% in SSP1–1.9 and SSP5–8.5, respectively, while no changes occur in the minimum value (around 25% in all three periods). As such, the NAO could exert a stronger control on European climate by the end of the century for some members.

The 5–95% range of uncertainty in both future patterns is largely similar in structure to that for the historical period, with comparable relative variations between the two NAO action centres (Fig. 3). Both the 95% patterns indicate a strengthening of the NAO, particularly of its southern centre of action which also shifts eastward, with an overall minor weakening of the northern pole, and a northward shift of the nodal line. Conversely, while the northern NAO pole deepens, the southern action centre weakens substantially and shifts westward in the 5% percentile patterns. The range of uncertainty in the future patterns is larger than the differences in the ensemble means, resulting in somewhat mixed patterns of change.

3.2.2. *Future changes in the response to the NAO*

Figure 4 shows the ensemble mean regression of R95p on the NAO index for the two future scenarios, along with the differences with

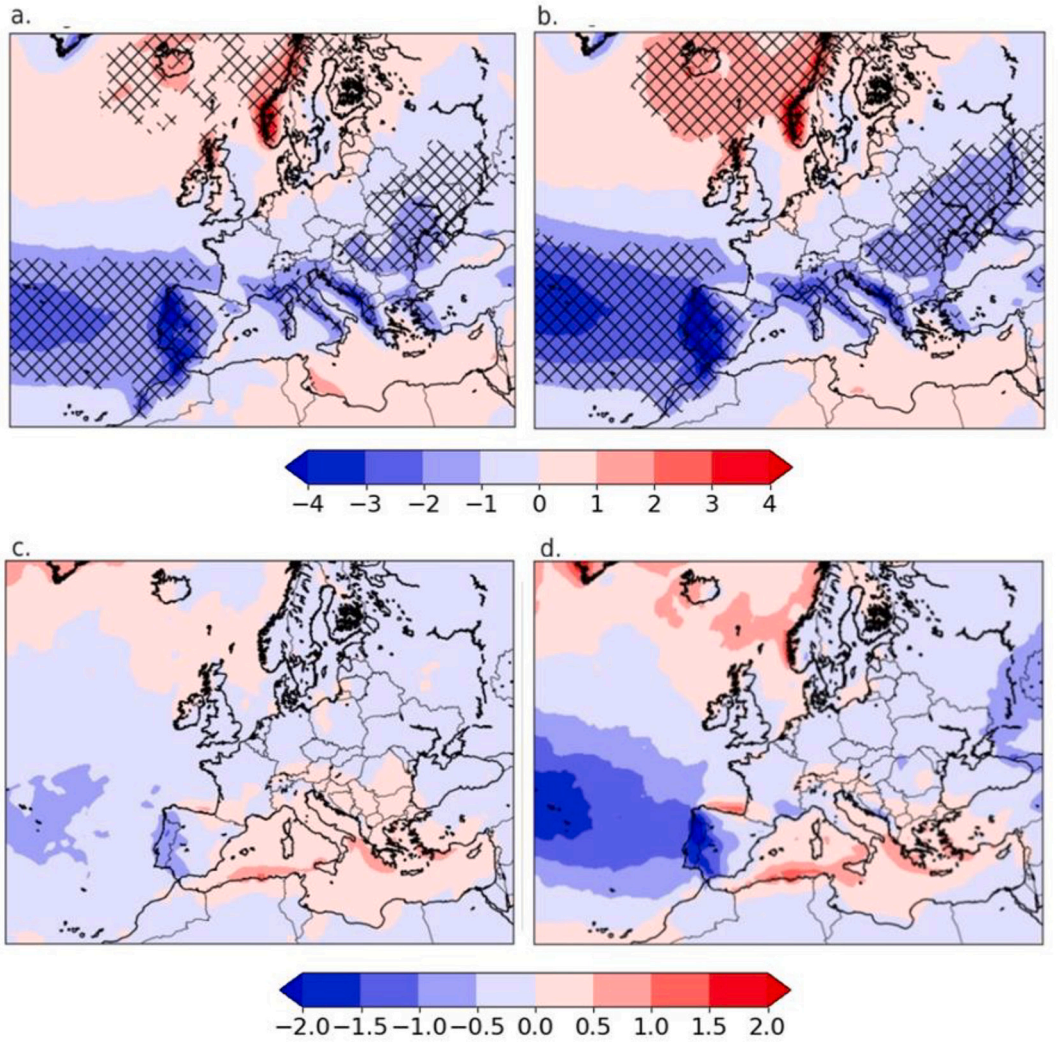

Fig. 4. Top: Future (2071–2100) DJFM R95p regressions (mm day^{-1}) on the NAO time series for the EC-Earth3 ensemble mean during 2071–2100 for (left) SSP1–1.9 and (right) SSP5–8.5. The cross-hatching marks regions where the correlation exceeds the 90% confidence level. Bottom: Differences (mm day^{-1}) between future and present-day DJFM R95p regressions on the NAO time series in the EC-Earth3 ensemble mean for (left) SSP1–1.9 and (right) SSP5–8.5.

respect to the present-day. The corresponding difference panels for R1xday and CDD are provided in Fig. 5. Magnitudes and spatial patterns of the future NAO-related anomalies are very similar, in their broad features, to the corresponding ones in the historical period. Again, the largest response to NAO variability within the Mediterranean region is found over Iberia, western Italy, and the Balkan coast. However, compared to present-day, the future NAO-related R95p anomalies across the Mediterranean Sea and most of the coastline are weaker (i.e., more extreme precipitation associated with the positive phase of the NAO), especially in SSP-1.19. Conversely, in both scenarios, the drying over Iberia further intensifies, particularly in SSP5–8.5 (up to 40% compared to present-day), as part of the large and extensive negative anomaly over the Atlantic. Although more spatially confined, particularly in SSP1–1.9, areas of larger negative anomalies (about 10%) are also found over southern France, northern and central Italy, and the Balkans. Widespread drying, albeit of modest magnitude, occurs over most of central and northern Europe. These changes are consistent with those in the NAO pattern discussed above, and are conducive to reduced westerly flow over western and central Europe and anomalous southwesterlies over the Mediterranean.

Changes in R1xday (Fig. S10) bear marked similarity to those in R95p. Projections of CDD (Fig. S10), compared to present-day, display a pattern of changes similar to that of the other two indices despite substantial differences in the underpinning climatology. Compared to the historical period, the NAO-related CDD regressions decrease in both future scenarios over the central and eastern Mediterranean, the Balkans, as well as over most of southern Europe, but increase over Iberia and central Europe (Fig. S10). The above results are indicative of an NAO-related future general wetting of the Mediterranean and the Balkans except over Spain and Portugal, which are subjected to further drying. Drying is also present over central Europe. Despite the broad similarities between the two scenarios, there are also noticeable differences: the NAO-related Mediterranean wetting in SSP5–8.5 is particularly large over the central basin compared to a broader and more uniform signal in SSP1–1.9.

Overall, the difference of the NAO-induced anomalies between SSP5–8.5 and SSP1–1.9 is comparable among the three precipitation indices (i.e., by comparing Fig. 4c and d, Fig. 5c and d) with local changes amounting to up to 20% of the present-day values. From this comparison, a quadrupole pattern of relative wetting over northwestern Europe and the central and eastern Mediterranean, and drying over south-western Europe and the Balkans emerges. The quadrupole can be related to the ensemble-mean differences in the NAO pattern between the two scenarios, and particularly the anomalous cyclone over central Europe and anticyclone over the mid-Atlantic in SSP5–8.5 compared to SSP1–1.9.

The inter-member variety of NAO patterns results in a corresponding range of extreme precipitation responses (Figs. S11 and S12). For example, simulations 12 in SSP1–1.9 and 15 in SSP5–8.5 feature larger negative R95p anomalies over the Atlantic and a weaker NAO signature over the continent compared to present-day which well correspond to the associated stronger and westward shifted NAO southern pole. Both scenarios include members with an overall very weak NAO signal (e.g., simulation 11 in SSP1–1.9 and 33 in SSP5–8.5), others with very large negative anomalies across the Mediterranean and central Europe (e.g., simulation 37 in SSP1–1.9 and 34 in SSP5–8.5). The difference between

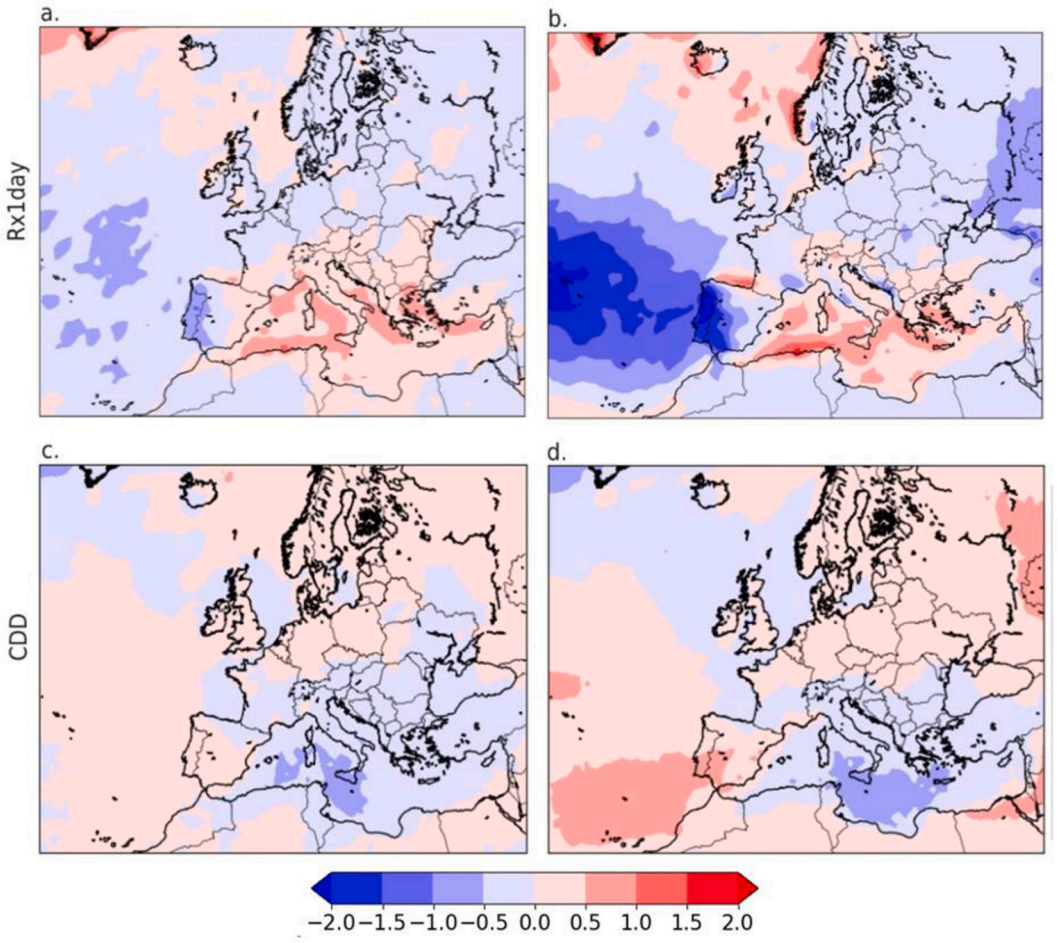

Fig. 5. Differences between future and present-day DJFM (top) Rx1day (mm day^{-1}) and (bottom) CDD (day) regressions on the NAO time series in the EC-Earth3 ensemble mean for (left) SSP1–1.9 and (right) SSP5–8.5.

future and present-day NAO-related R95p patterns for each ensemble member reveals a large degree of uncertainty in sign and magnitude of the projected changes across the Euro-Mediterranean region. Some members display almost muted changes (e.g., simulation 36 in SSP1–1.9 and 47 in SSP5–8.5), while others changes consistent with present-day anomalies (e.g., simulation 20 in SSP1–1.9 and simulation 14 in SSP5–8.5).

The range of future NAO-related R95p anomalies is remarkably similar in terms of magnitude and spatial pattern between the two future scenarios (Fig. 6) as well as compared to the present-day ones (Fig. S5). Projected anomalies can change sign with respect to the present-day mean over most of the domain, particularly over the Mediterranean region, as shown by comparing the 5–95% range of future R95p anomalies (Fig. 6) with the present-day mean (Fig. 1d). For example, for the countries bordering the Mediterranean Sea, changes can range from 1.5 mm day^{-1} or more to −1.5 mm day^{-1} in both scenarios, with sub-regional values even much larger than those (e.g., over southern France and northern Italy, western Greece, and northern Portugal). These spreads in future variations are consistent with those in the related NAO patterns discussed above. Interestingly, while the broad-scale features of the range of spatial patterns are similar in the two scenarios, there are also important sub-regional differences: for example, both the 5% and the 95% patterns feature more negative values over southern Europe, and Iberia in particular, in SSP5–8.5 than in SSP1–1.9. Opposite responses occur over most of central and northern Europe. Similar findings hold for Rx1day, but with a larger uncertainty range across the Mediterranean (compare Fig. S13 with Fig. 2). In contrast, the pattern of the 5–95% range of uncertainty of future CDD changes in SSP5–8.5 features (positive) values between +1.5 days over Iberia and + 0.6–0.8 days over the central and eastern Mediterranean at the upper tail, and approximately opposite (and negative) values at the 5% threshold. Values in SSP1–1.9 are consistently 0.5–1 day larger than those for SSP5–8.5 (Fig. S14 and Fig. 2).

3.3. Quantification of the contribution of internal variability

The above results provide a qualitative depiction of the range of magnitudes and spatial patterns of projected NAO-related changes in precipitation extremes due to a combination of external radiative forcing and internal climate variability.

Figure 7 shows that internal variability plays a major role in the NAO-related changes of R95p for most of the areas surrounding the Mediterranean Sea and central Europe. In this region, internal variability provides on average a contribution of up to 90% or more to the total variability in SSP1–1.9, and of about 80% in SSP5–8.5. Correspondingly, the SNR is around 0.2 over the large majority of the domain in both scenarios (Fig. S15). The only exceptions are some areas across the Mediterranean Sea and a larger region in the Atlantic extending over central and western Iberia, where external forcing can contribute about 30–40% or more to the projected changes (SNR >0.5). In this respect, the central and western Iberian Peninsula is the area with the largest anthropogenic signature across the whole domain (exceeding 50% in SSP5–8.5, SNR larger than 1). The spatial patterns of IV (SNR) are largely similar in the two scenarios and consistent with those of the forced responses over both the Mediterranean only and the larger European domain, with a negligible influence from the underlying global

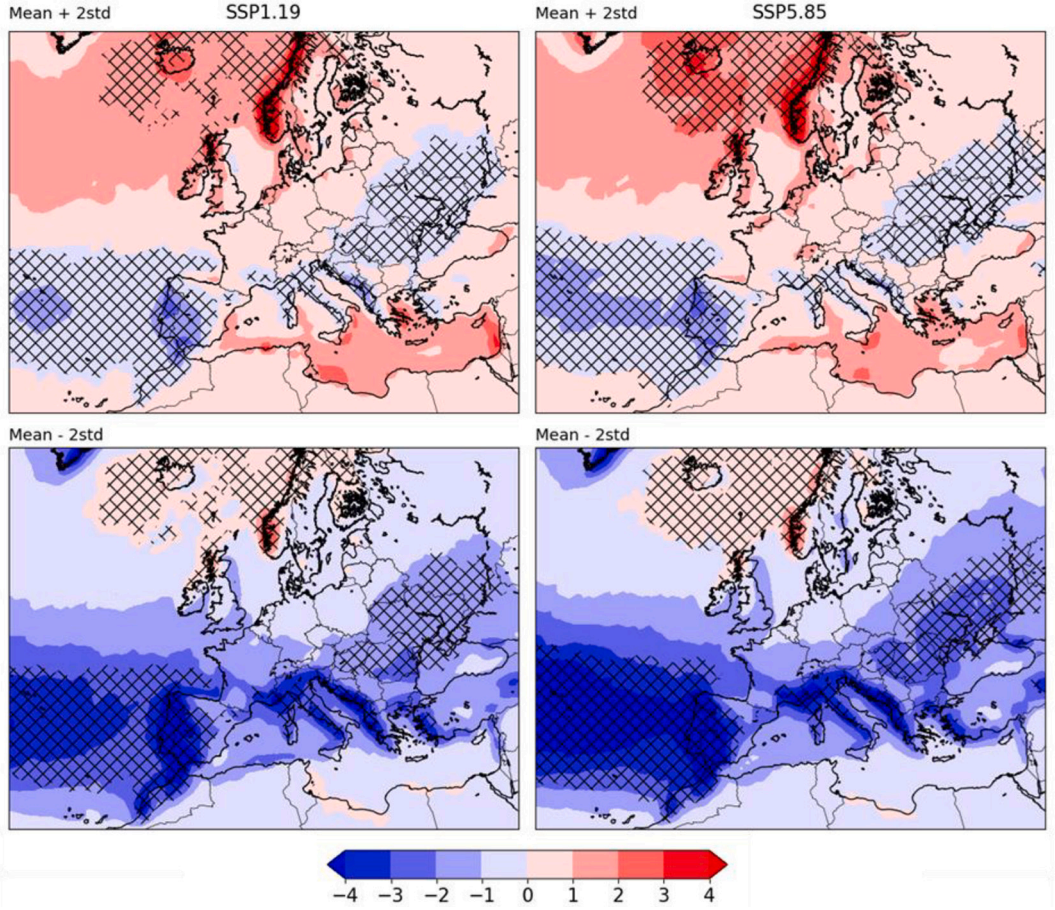

Fig. 6. The 5–95% range of the simulated DJFM R95p regressions on the NAO time series for the EC-Earth3 ensemble mean during 2071–2100 for (left) SSP1–1.9 and (right) SSP5–8.5. Top: the 95% (mean + 2 inter-member standard deviations). Bottom: the 5% (mean - 2 inter-member standard deviations). The cross-hatching marks regions where the correlation exceeds the 90% confidence level.

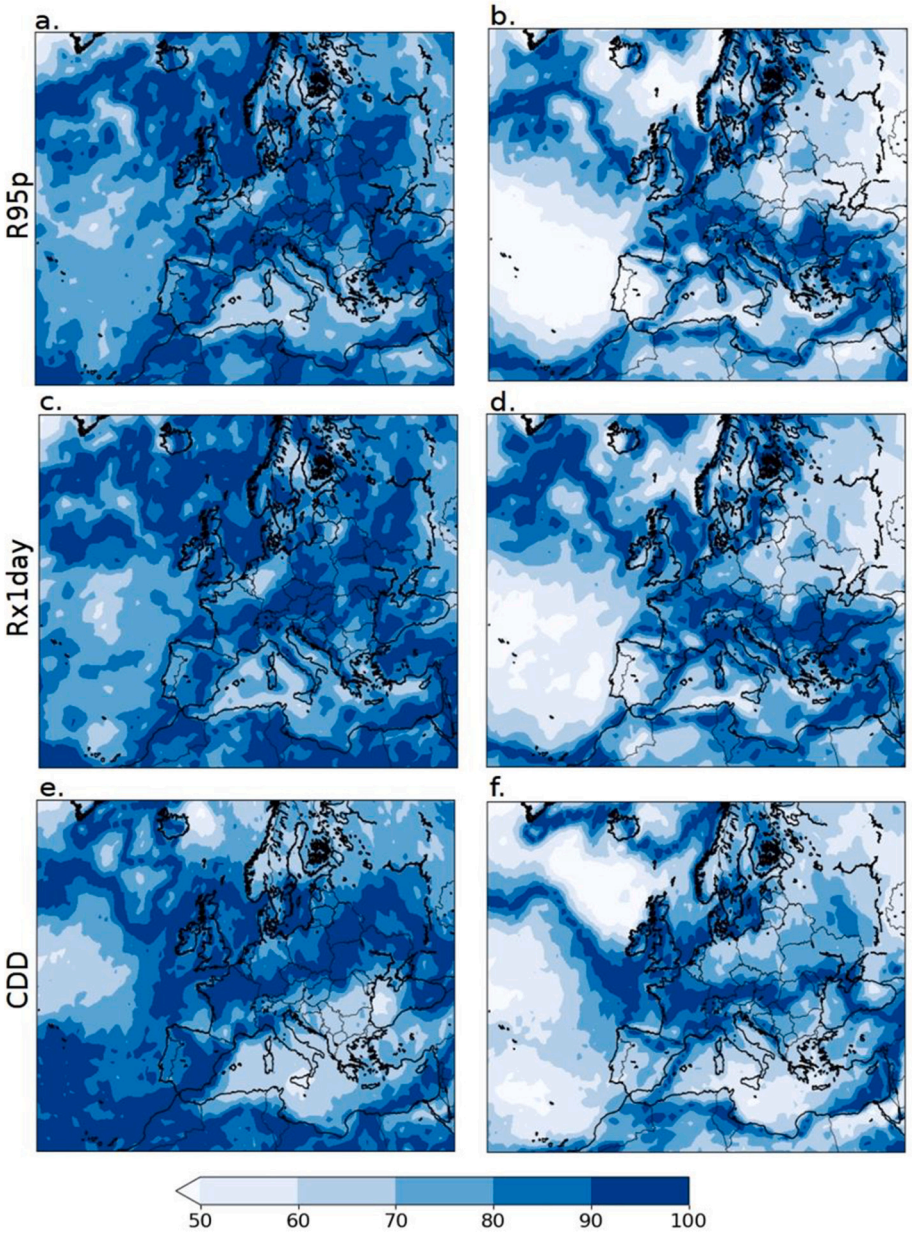

Fig. 7. Relative contribution of internal variability (%) to the changes in (top to bottom) R95p, Rx1day, CDD between (2071–2100) and present-day for (left) SSP1–1.9 and (right) SSP5–8.5. See text for the equation used.

warming level (spatial correlation around 0.85 in all cases). This suggests internal variability to be the primary driver of the magnitude of future changes, with external forcing playing a key role in determining their spatial pattern. While the anthropogenic signal is more discernible in SSP5–8.5 than in SSP1–1.9, especially over Iberia, southern France and northern Italy (+15–20%), as well as over northeastern Europe (+25%), there are also areas where its contribution decreases despite the larger global warming, such as across northern France and northern Germany and parts of the eastern Mediterranean (about 10–15%). Very similar conclusions hold also for changes in Rx1day. A close examination of the spatial patterns reveals a smaller contribution of internal variability (5–10% on average) compared to R95p in SSP1–1.9 over the Mediterranean, while conversely, internal variability is more predominant (15%) over Iberia. Externally-driven changes are however less important (10% on average) for Rx1day compared to R95p in SSP5–8.5 over most of the western regions. While overall internal variability also dominates the changes in CDD, there are also important differences compared to the previous two indices. For example, in SSP1–1.9 the contribution of internal variability is particularly large (90%) over the Iberian Peninsula (where, conversely, it is much lower for R95p), while it drops to about 70% over the central and eastern Mediterranean and the Balkans (as opposed to that for R95p). In SSP5–8.5, despite the further warming, the anthropogenic signal increases over the Iberian Peninsula (by about 30%) and parts of the central Mediterranean Sea, while it decreases, albeit only modestly, over the rest of the Mediterranean domain. This further attests to the predominant role of internal variability and emphasises that the externally-forced signal may have a different role for different indices and over different regions.

4. Summary and concluding remarks

This study investigates the influence of NAO variability on precipitation extremes over the Mediterranean region during the boreal winter at present-day, and how this relationship might change at the end of the

21st century under two different emission pathways associated with spatio-temporal changes in the NAO. Using the EC-Earth3 large ensemble experiments allows us to characterise the role of external forcing and internal variability more robustly by averaging over the 50 ensemble members. This topic is of utmost importance yet largely unexplored.

The NAO exerts an important impact on the intensity of winter rainfall extremes in the Mediterranean, with good agreement between model and observations. Specifically, the NAO is anti-correlated with extreme precipitation intensity and positively correlated with the persistence of dry conditions across the region, consistent with its link with average winter climate across the Euro-Mediterranean region. The impact of NAO variability is not homogenous across the basin, and the strongest influence is observed over Iberia, western Italy, the Balkan coast and the Aegean Sea. In these areas, the NAO variability explains 5–20% of the monthly total variance of R95p and Rx1day and produces variations between 20 and 60% of the climatology. For CDD, the strongest NAO influence is over southern Spain, the Balkan coast, and the Aegean Sea. On a Mediterranean-wide scale, the NAO variability explains a slightly more significant fraction of variance for CDD than for R95p and Rx1day.

At the end of the 21st century, significant changes in intensity and variance of all the studied precipitation indices are projected in both SSP1–1.9 and SSP5–8.5 across the Mediterranean domain (Figs. S16 and S17), with similar magnitudes across the indices. In both scenarios, an opposite pattern of change applies to R95p and Rx1day compared to CDD: an increase (decrease) in intensity and variance is projected for the former two (latter) from northern Europe to the central Mediterranean, while the opposite occurs across the north African coast.

Despite the future changes in R95p, Rx1day, and CDD total intensity and variance, the influence of NAO variability does not appreciably vary in the future. While marked local differences in magnitude and spatial patterns exist, such as over the Iberian Peninsula and parts of the central Mediterranean, they are overall of modest magnitude when considering basin-wide changes. In general, the NAO-related extreme precipitation anomalies are very similar to present-day in both SSP1–1.9 and SSP5–8.5. Subtracting the externally-forced component from the SSP1–1.9 and SSP5–8.5 simulations does not produce significant changes in the area-averaged regressions. This highlights the role of internal variability, and the spread in the circulation responses to different levels of warming, in determining the impact of the NAO. While the irreducible uncertainty associated with internal variability dominates the future NAO-related precipitation extremes across the Mediterranean, the link with the NAO is nonetheless crucial as it provides large-scale spatial organization to the otherwise uncoherent circulation variability and associated climate response. These findings provide further support to recent works (e.g., Deser et al., 2017; McKenna and Maycock, 2021, 2022), which also noted the large spread in the NAO circulation response to global warming. This study is however the first to use state-of-the-art large ensemble simulations and scenarios to investigate the NAO imprint on precipitation extremes.

An important implication follows for the interpretation of the drivers of precipitation extremes over Southern Europe. On one hand, these results suggest that the NAO will explain a lower percentage of winter extreme precipitation variance across the Mediterranean, as only minimal changes in the NAO correlation to R95p and Rx1day are detected despite a strong increase in their total variance. Accordingly, the NAO variability will have a lower relative impact on the intensity of extreme precipitation, as the magnitude of R95p and Rx1day regressions on the NAO index does not change despite the net increase in the intensity of these indices between the future and the historical scenarios. As for R95p and Rx1day, the NAO will exert a weaker influence on CDD across the southern Mediterranean (south of 39°N), where both CDD duration and variance significantly increase. However, the opposite applies to the northern Mediterranean (north of 39°N), where a reduction in CDD duration and variance is projected in both emission scenarios. This reduction is particularly significant in the SSP1–1.9 scenario, in which 10% decreases in CDD duration are projected across the entire Mediterranean domain. Hence, in a low-warming emission scenario, the NAO might exert a stronger control on winter CDD across the Mediterranean than in the past.

Although this study makes use of a large ensemble, the results will need to be confirmed by the analysis of other large single-model ensembles as well as of the new CMIP6 experiments. More specifically, this may also help to investigate the influence of model shortcomings in the simulated NAO and precipitation extremes features and their link. Given the strong influence of model physics and physical parameterizations, including model resolution, on precipitation processes, a multi-model approach is critical to achieving more robust results. Further investigations should also take into consideration, for example, inter-model differences in simulating the present-day and future NAO characteristics (McKenna and Maycock, 2022). Several Mediterranean countries rank as the most affected in Europe by the damages of weather-related hazards over the last forty years relative to their population and GDP (EEA, 2022). Thus, a more robust identification of the factors affecting future changes in weather extremes would represent a major leap forward in our understanding of climate change impacts, leading to radical improvements in current mitigation and adaptation strategies (Trenberth, 2012; Hulme, 2014).

CRediT authorship contribution statement

Andrea Rivosecchi: Writing – original draft, Visualization, Formal analysis. **M.A. Bollasina:** Writing – review & editing, Supervision, Conceptualization. **I. Colfescu:** Writing – review & editing.

Declaration of competing interest

The authors declare that they have no known competing financial interests or personal relationships that could have appeared to influence the work reported in this paper.

Data availability

EC-Earth3 data are available at https://esgf-node.llnl.gov/projects/esgf-llnl/. The ERA-I monthly data are obtained at https://www.ecmwf.int/en/forecasts/datasets/reanalysis-datasets/era-interim. The E-OBS dataset is accessed from https://www.ecad.eu/download/ensembles/download.php.

Acknowledgements

MAB acknowledges support from the Natural Environment Research Council (NE/N006038/1).

Appendix A. Supplementary data

Supplementary data to this article can be found online at https://doi.org/10.1016/j.atmosres.2024.107391.

References

Alpert, P.T., Ben-gai, A., Baharad, Y., Benjamini, D., et al., 2002. The paradoxical increase of Mediterranean extreme daily rainfall in spite of decrease in total values. Geophys. Res. Lett. 29 https://doi.org/10.1029/2001GL013554.

Ballinger, A.P., Schurer, A.P., O'Reilly, C.H., Hegerl, G.C., 2023. The importance of accounting for the North Atlantic Oscillation when applying observational constraints to European climate projections. Geophys. Res. Lett. 50, e2023GL103431 https://doi.org/10.1029/2023GL103431.

Blanusa, M.L., López-Zurita, C.J., Rasp, S., 2023. Internal variability plays a dominant role in global climate projections of temperature and precipitation extremes. Clim. Dyn. 61, 1931–1945. https://doi.org/10.1007/s00382-023-06664-3.

Castro-Díez, Y., Pozo-Vázquez, D., Rodrigo, F.S., Esteban-Parra, M.J., 2002. NAO and winter temperature variability in southern Europe. Geophys. Res. Lett. 29 https://doi.org/10.1029/2001GL014042.

Chen, H., Sun, J., Chen, X., 2014. Projection and uncertainty analysis of global precipitation-related extremes using CMIP5 models. Int. J. Climatol. 34, 2730–2748. https://doi.org/10.1002/joc.3871.
Cornes, R.C., van der Schrier, G., van den Besselaar, E.J.M., Jones, P.D., 2018. An ensemble version of the E-OBS temperature and precipitation data sets. J. Geophys. Res. 123, 9391–9409. https://doi.org/10.1029/2017JD028200.
Corona, R., Montaldo, N., Albertson, J.D., 2018. On the role of NAO-driven interannual variability in rainfall seasonality on water resources and hydrologic design in a typical Mediterranean basin. J. Hydrometeorol. 19, 485–498. https://doi.org/10.1175/JHM-D-17-0078.1.
Cos, J., Doblas-Reyes, F., Jury, M., Marcos, R., Bretonnière, P.-A., Samsó, M., 2022. The Mediterranean climate change hotspot in the CMIP5 and CMIP6 projection. Earth Syst. Dynam. 13, 321–340. https://doi.org/10.5194/esd-13-321-2022.
Cramer, W., Guiot, J., et al., 2018. Climate change and interconnected risks to sustainable development in the Mediterranean. Nat. Clim. Chang. 8, 972–980. https://doi.org/10.1038/s41558-018-0299-2.
Deser, C., Phillips, A., Bourdette, V., Teng, H., 2012. Uncertainty in climate change projections: the role of internal variability. Clim. Dyn. 38, 527–546. https://doi.org/10.1007/s00382-010-0977-x.
Deser, C., Terray, L., Phillips, A.S., 2016. Forced and internal components of winter air temperature trends over North America during the past 50 years: mechanisms and implications. J. Clim. 29, 2237–2258. https://doi.org/10.1175/JCLI-D-15-0304.1.
Deser, C., Hurrell, J.W., Phillips, A.S., 2017. The role of the North Atlantic Oscillation in European climate projections. Clim. Dyn. 49, 3141–3157. https://doi.org/10.1007/s00382-016-3502-z.
Deser, C., et al., 2020. Insights from Earth system model initial-condition large ensembles and future prospects. Nat. Clim. Chang. 10, 277–286. https://doi.org/10.1038/s41558-020-0731-2.
Döscher, R., Acosta, M., et al., 2022. The EC-Earth3 Earth system model for the coupled Model Intercomparison Project 6. Geosci. Model Dev. 15, 2973–3020. https://doi.org/10.5194/gmd-15-2973-2022.
Dünkeloh, A., Jacobeit, J., 2003. Circulation dynamics of Mediterranean precipitation variability 1948–98. Int. J. Climatol. 23, 1843–1866. https://doi.org/10.1002/joc.973.
EEA, 2022. Economic Losses and Fatalities from Weather- and Climate-related Events in Europe. Report of the European Environment Agency. available here: https://www.eea.europa.eu/publications/economic-losses-and-fatalities-from.
Fabiano, F., Meccia, V.L., Davini, P., Ghinassi, P., Corti, S., 2021. A regime view of future atmospheric circulation changes in northern mid-latitudes. Weather Clim. Dynam. 2, 163–180. https://doi.org/10.5194/wcd-2-163-2021.
Fereday, D., Chadwick, R., Knight, J., Scaife, A.A., 2018. Atmospheric dynamics is the largest source of uncertainty in future winter European rainfall. J. Clim. 31, 963–977. https://doi.org/10.1175/JCLI-D-17-0048.1.
Ferrari, E., Caloiero, T., Coscarelli, R., 2013. Influence of the North Atlantic Oscillation on winter rainfall in Calabria (southern Italy). Theor. Appl. Climatol. 114, 479–494. https://doi.org/10.1007/s00704-013-0856-6.
Fischer, E.M., Knutti, R., 2016. Observed heavy precipitation increase confirms theory and early models. Nat. Clim. Chang. 6, 986–991. https://doi.org/10.1038/nclimate3110.
Garcia-Martinez, I.M., Bollasina, M.A., 2021. Identifying the evolving human imprint on heat wave trends over the United States and Mexico. Environ. Res. Lett. 16, 094039 https://doi.org/10.1088/1748-9326/ac1edb.
Gillett, N.P., Fyfe, J.C., 2013. Annular mode changes in the CMIP5 simulations. Geophys. Res. Lett. 40, 1189–1193. https://doi.org/10.1002/grl.50249.
Giorgi, F., Lionello, P., 2008. Climate change projections for the Mediterranean region. Glob. Planet. Chang. 63, 90–104. https://doi.org/10.1016/j.gloplacha.2007.09.005.
Giorgi, F., Coppola, E., Raffaele, F., 2014. A consistent picture of the hydroclimatic response to global warming from multiple indices: models and observations. J. Geophys. Res. 119 https://doi.org/10.1002/2014JD022238.
Hersbach, H., Bell, B., Berrisford, P., et al., 2020. The ERA5 global reanalysis. Q.J.R. Meteorol. Soc. 146, 1999–2049. https://doi.org/10.1002/qj.3803.
Houssos, E.E., Bartzokas, A., 2006. Extreme precipitation events in NW Greece. Adv. Geosci. 7, 91–96. https://doi.org/10.5194/adgeo-7-91-2006.
Hulme, M., 2014. Attributing weather extremes to climate change: a review. Prog. Phys. Geogr. 38, 499–511. https://doi.org/10.1177/0309133314538644.
Hurrell, J.W., 1995. Decadal trends in the North Atlantic Oscillation: regional temperatures and precipitation. Science 269, 676–679. https://doi.org/10.1126/science.269.5224.676.
Hurrell, J.W., Deser, C., 2010. North Atlantic climate variability: the role of the North Atlantic Oscillation. J. Mar. Syst. 79, 231–244. https://doi.org/10.1016/j.jmarsys.2009.11.002.
IPCC, Masson-Delmotte, V., Zhai, P., Pirani, A., Connors, S.L., Péan, C., Berger, S., Caud, N., Chen, Y., Goldfarb, L., Gomis, M.I., Huang, M., Leitzell, K., Lonnoy, E., Matthews, J.B.R., Maycock, T.K., Waterfield, T., Yelekçi, O., Yu, R., Zhou, B., 2021. Climate Change 2021: The Physical Science Basis. Contribution of Working Group I to the Sixth Assessment Report of the Intergovernmental Panel on Climate Change. Cambridge University Press, Cambridge, United Kingdom and New York, NY, USA. https://doi.org/10.1017/9781009157896.
Jung, T., Hilmer, M., Ruprecht, E., Kleppek, S., Gulev, S.K., Zolina, O., 2003. Characteristics of the recent eastward shift of interannual NAO variability. J. Clim. 16 https://doi.org/10.1175/1520-0442(2003)016<3371:COTRES>2.0.CO;2.
Kelley, C., Ting, M., Seager, R., et al., 2012. The relative contributions of radiative forcing and internal climate variability to the late 20th Century winter drying of the Mediterranean region. Clim. Dyn. 38, 2001–2015. https://doi.org/10.1007/s00382-011-1221-z.
King, A., Karoly, D., 2017. Climate extremes in Europe at 1.5 and 2 degrees of global warming. Environ. Res. Lett. 12, 114031 https://doi.org/10.1088/1748-9326.
Knippertz, P., Christoph, M., Speth, P., 2003. Long-term precipitation variability in Morocco and the link to the large-scale circulation in recent and future climates. Meteorog. Atmos. Phys. 83, 67–88. https://doi.org/10.1007/s00703-002-0561-y.
Kravtsov, S., 2017. Pronounced differences between observed and CMIP5-simulated multidecadal climate variability in the twentieth century. Geophys. Res. Lett. 44, 5749–5757. https://doi.org/10.1002/2017GL074016.
Krichak, S.O., Breitgand, J.S., Gualdi, S., Feldstein, S.B., 2014. Teleconnection-extreme precipitation relationships over the Mediterranean region. Theor. Appl. Climatol. 117, 679–692. https://doi.org/10.1007/s00704-013-1036-4.
Lee, J.-Y., et al., 2021. Future Global climate: Scenario-based Projections and Near-Term Information. In: Climate Change 2021: The Physical Science Basis. Contribution of Working Group I to the Sixth Assessment Report of the Intergovernmental Panel on Climate Change. Cambridge University Press, Cambridge, United Kingdom and New York, NY, USA, pp. 553–672. https://doi.org/10.1017/9781009157896.006.
Lehner, F., Deser, C., Maher, N., et al., 2020. Partitioning climate projection uncertainty with multiple large ensembles and CMIP5/6. Earth Syst. Dynam. 11 https://doi.org/10.5194/esd-11-491-2020.
Lopez-Moreno, J.I., Vicente-Serrano, S.M., Morán-Tejeda, E., Lorenzo-Lacruz, J., Kenawy, A., Beniston, M., 2011. Effects of the North Atlantic Oscillation (NAO) on combined temperature and precipitation winter modes in the Mediterranean mountains: observed relationships and projections for the 21st century. Glob. Planet. Chang. 77, 62–76. https://doi.org/10.1016/j.gloplacha.2011.03.003.
Luo, D.H., Yao, Y., Dai, A.G., Feldstein, S.B., 2015. The positive North Atlantic Oscillation with downstream blocking and Middle East snowstorms: the large-scale environment. J. Clim. 28, 6398–6418. https://doi.org/10.1175/JCLI-D-15-0184.1.
Luppichini, M., Barsanti, M., Giannecchini, R., Bini, M., 2021. Statistical relationships between large-scale circulation patterns and local-scale effects: NAO and rainfall regime in a key area of the Mediterranean basin. Atmos. Res. 248 https://doi.org/10.1016/j.atmosres.2020.105270.
Madsen, H., Lawrence, D., Lang, M., Martinkova, M., Kjeldsen, T.R., 2014. Review of trend analysis and climate change projections of extreme precipitation and floods in Europe. J. Hydrol. 519, 3634–3650. https://doi.org/10.1016/j.jhydrol.2014.11.003.
McKenna, C.M., Maycock, A.C., 2021. Sources of uncertainty in Multimodel large Ensemble projections of the winter North Atlantic Oscillation. Geophys. Res. Lett. 48, e2021GL093258 https://doi.org/10.1029/2021GL093258.
McKenna, C.M., Maycock, A.C., 2022. The role of the North Atlantic Oscillation for projections of winter mean precipitation in Europe. Geophys. Res. Lett. 49, e2022GL099083 https://doi.org/10.1029/2022GL099083.
Myhre, G., Alterskjær, K., Stjern, C.W., et al., 2019. Frequency of extreme precipitation increases extensively with event rareness under global warming. Sci. Rep. 9 https://doi.org/10.1038/s41598-019-52277-4.
Nigam, S., Baxter, S., 2015. General circulation of the atmosphere: teleconnections. In: Encycl. Atmos. Sci. 2nd edn 3, 90–109. https://doi.org/10.1016/B978-0-12-382225-3.00400-X.
O'Neill, B.C., Kriegler, E., et al., 2014. A new scenario framework for climate change research: the concept of shared socioeconomic pathways. Clim. Chang. 122, 387–400. https://doi.org/10.1007/s10584-013-0905-2.
O'Reilly, C.H., Befort, D.J., Weisheimer, A., et al., 2021. Projections of northern hemisphere extratropical climate underestimate internal variability and associated uncertainty. Commun. Earth. Environ. 2, 194. https://doi.org/10.1038/s43247-021-00268-7.
Pfahl, S., O'Gorman, P.A., Fischer, E.M., 2017. Understanding the regional pattern of projected future changes in extreme precipitation. Nat. Clim. Chang. 7, 423–427. https://doi.org/10.1038/nclimate3287.
Polade, S.D., Gershunov, A., Cayan, D.R., Dettinger, M.D., Pierce, D.W., 2017. Precipitation in a warming world: assessing projected hydro-climate changes in California and other Mediterranean climate regions. Sci. Rep. 7, 1–10. https://doi.org/10.1038/s41598-017-11285-y.
Queralt, S., Hernández, E., Barriopedro, D., Gallego, D., Ribera, P., Casanova, C., 2009. North Atlantic Oscillation influence and weather types associated with winter total and extreme precipitation events in Spain. Atmos. Res. 94, 675–683. https://doi.org/10.1016/j.atmosres.2009.09.005.
Rousi, E., Ulbrich, U., Rust, H.W., Anagnostolpoulou, C., 2017. An NAO climatology in reanalysis data with the use of self-organizing maps. In: Karacostas, T., Bais, A., Nastos, P.T. (Eds.), Perspectives on Atmospheric Sciences. Springer. https://doi.org/10.1007/978-3-319-35095-0_103.
Rousi, E., Rust, H.W., Ulbrich, U., Anagnostopoulou, C., 2020. Implications of winter NAO flavors on present and future European climate. Climate 8. https://doi.org/10.3390/cli8010013.
Sassi, S., Nicotina, L., Pall, P., Stone, D., Jewson, S., 2019. Impact of climate change on European winter and summer flood losses. Adv. Water Resour. 129, 165–177. https://doi.org/10.1016/j.advwatres.2019.05.014.
Shepherd, T.G., 2014. Atmospheric circulation as a source of uncertainty in climate change projections. Nat. Geosci. 7, 703–708. https://doi.org/10.1038/ngeo2253.
Sillmann, J., Kharin, B., Zwiers, F., Zhang, X., Bronaugh, D., 2013. Climate extreme indices in the CMIP5 multi-model ensemble. Part 2: future projections. J. Geophys. Res. https://doi.org/10.1002/jgrd.50188.
Smith, D.M., et al., 2020. North Atlantic climate far more predictable than models imply. Nature 583. https://doi.org/10.1038/s41586-020-2525-0.
Suarez-Gutierrez, L., Li, C., Müller, W.A., Marotzke, J., 2018. Internal variability in European summer temperatures at 1.5°C and 2°C of global warming. Environ. Res. Lett. 13 https://doi.org/10.1088/1748-9326/aaba58.

Svetlana, D., Radovan, D., Ján, D., 2015. The economic impact of floods and their importance in different regions of the world with emphasis on Europe. Proc. Econ. Finance. 34, 649–655. https://doi.org/10.1016/S2212-5671(15)01681-0.

Tao, L., Fang, J., Yang, X.-Q., Sun, X., Cai, D., Wang, Y., 2023. Role of North Atlantic tripole SST in mid-winter reversal of NAO. Geophys. Res. Lett. 50 https://doi.org/10.1029/2023GL103502.

Tomozeiu, R., Lazzeri, M., Cacciamani, C., 2002. Precipitation fluctuations during the winter season from 1960 to 1995 over Emilia-Romagna, Italy. Theor. Appl. Climatol. 72, 221–229. https://doi.org/10.1007/s00704-002-0675-7.

Tramblay, Y., Badi, W., Driouech, F., el Adlouni, S., Neppel, L., Servat, E., 2012. Climate change effects on extreme precipitation events in Morocco. Glob. Planet. Chang. 82–83 https://doi.org/10.1016/j.gloplacha.2011.12.002.

Trenberth, K.E., 2012. Framing the way to relate climate extremes to climate change. Clim. Chang. 115, 283–290. https://doi.org/10.1007/s10584-012-0441-5.

Trigo, R.M., Pozo-Vázquez, D., Osborn, T.J., Castro-Díez, Y., Gámiz-Fortis, S., Esteban-Parra, M.J., 2004. North Atlantic Oscillation influence on precipitation, river flow and water resources in the Iberian Peninsula. Int. J. Climatol. 24, 925–944. https://doi.org/10.1002/joc.1048.

Tuel, A., Eltahir, E.A.B., 2020. Why is the Mediterranean a climate change hot spot? J. Clim. 33, 5829–5843. https://doi.org/10.1175/JCLI-D-19-0910.1.

Tuel, A., O'Gorman, P.A., Eltahir, E.A.B., 2021. Elements of the dynamical response to climate change over the Mediterranean. J. Clim. 34, 1135–1146. https://doi.org/10.1175/JCLI-D-20-0429.1.

Vautard, R., Gobiet, A., Sobolowski, S., Kjellström, E., Stegehuis, A., Watkiss, P., Mendlik, T., Landgren, O., Nikulin, G., Teichmann, C., Jacob, D., 2014. The European climate under a 2 C global warming. Environ. Res. Lett. 9 https://doi.org/10.1088/1748-9326/9/3/034006.

Visbeck, M.H., Hurrell, J.W., Polvani, L., Cullen, H.M., 2001. The North Atlantic Oscillation: past, present, and future. Proc. Natl. Acad. Sci. USA 98, 12876–12877. https://doi.org/10.1073/pnas.231391598.

Wallace, J.M., Deser, C., Smoliak, B., Phillips, A.S., 2013. Attribution of climate change in the presence of internal variability. In: Climate Change: Multidecadal and Beyond. World Scientific Series on Asia-Pacific Weather and Climate, pp. 1–29. https://doi.org/10.1142/9789814579933_0001.

Wood, R.R., Ludwig, R., 2020. Analyzing internal variability and forced response of subdaily and daily extreme precipitation over Europe. Geophys. Res. Lett. 47 https://doi.org/10.1029/2020GL089300.

Yao, Y., Luo, D.H., Dai, A.G., Feldstein, S.B., 2016. The positive North Atlantic Oscillation with downstream blocking and Middle East snowstorms: Impacts of the North Atlantic jet. J. Clim. 29, 1853–1876. https://doi.org/10.1175/JCLI-D-15-0350.1.

Yu, B., Li, G., Chen, S., Lin, H., 2020. The role of internal variability in climate change projections of north American surface air temperature and temperature extremes in CanESM2 large ensemble simulations. Clim. Dyn. 55, 869–885. https://doi.org/10.1007/s00382-020-05296-1.

Zappa, G., Shepherd, T.G., 2017. Storylines of atmospheric circulation change for European regional climate impact assessment. J. Clim. 30, 6561–6577. https://doi.org/10.1175/JCLI-D-16-0807.1.

Zappa, G., Hoskins, B.J., Shepherd, T.G., 2015. The dependence of wintertime Mediterranean precipitation on the atmospheric circulation response to climate change. Environ. Res. Lett. 10, 104012 https://doi.org/10.1088/1748-9326/10/10/104012.

Zhang, X., Alexander, L., et al., 2011. Indices for monitoring changes in extremes based on daily temperature and precipitation data. WIREs Clim. Change. 2, 851–870. https://doi.org/10.1002/wcc.147.

Zittis, G., Bruggeman, A., Lelieveld, J., 2021. Revisiting future extreme precipitation trends in the Mediterranean. Weather Clim. Extrem. 34 https://doi.org/10.1016/j.wace.2021.100380.